Silver nanocluster in zeolites. ADSORPTION of ETHYLENE traces for fruit preservation

Larisha Cisneros[a],[1], Fei Gao[b],[**], Avelino Corma[a],[*]

[a] *Instituto de Tecnología Química, Universitat Politècnica de València -Consejo Superior de Investigaciones Científicas, Avda. de los Naranjos s/n, 46022, Valencia, Spain*
[b] *Jiangsu Key Laboratory of Vehicle Emissions Control, School of Environment, Center of Modern Analysis, Nanjing University 22, Hankou Road, 210093, Nanjing, PR China*

ARTICLE INFO

ABSTRACT

Removal of trace amounts of C_2H_4 from air streams at low temperature is technologically important for fruit preservation in warehouses. For that reason, a systematic quantitative and comparative study of Ag-zeolites for trace ethylene adsorption has been carried out. Combining characterization results with trace ethylene adsorption in a fixed-bed system have allowed to stablish a correlation between $Ag^{\delta+}$ species present in the zeolites and trace ethylene adsorption capacity. Among the zeolites studied, silver exchanged zeolites with -CHA (SSZ-13) and -LTA (5A) frameworks exhibited the most stable and highly dispersed silver sites, with an excellent potential for indoor environmental control of trace ethylene at 0 °C.

1. Introduction

Ripening is a metabolism process in fruits, vegetables, and cut flowers that causes most of the fruits to become sweeter, less green and softer and more edible. It is well known that the metabolism can be minimized by lowering the temperature and oxygen reduction. Whereas, in climacteric fruits and vegetables, the metabolism will be accelerated by the presence of low concentrations of ethylene (C_2H_4) emission from the storefruits [1]. Continued and uncontrolled biochemical activity caused by ethylene, subsequent to ripening leads to rotting of fruits and vegetables, and render them unfit for consumption [2]. Therefore, preventing deterioration or spoilage of fruits and vegetables during transportation and storage is of paramount importance and for doing that, it becomes important to eliminate trace ethylene (with ppm level) in the streams of air at low temperature (ca. 0–4 °C).

One elegant procedure to eliminate C_2H_4 could be to recirculate the air within the chamber through a catalytic bed inwhere a catalyst would oxidize the C_2H_4 to CO_2 and H_2O. Unfortunately, hydrocarbon oxidation catalysts normally operate at higher temperature (200–300 °C) [3–7], and this process will require heating the air from the usual temperature (2–5 °C) in the chambers to 200–300 °C and then cooling down again. It is clear, that the described oxidation process will be too energy-intensive system [8], and today existing catalysts have insufficient activity [7,9,10] or poor stability

[11] for working at low temperature for the complete ethylene oxidation. Besides destructive techniques based on the removal of ethylene by oxidation, the recuperative techniques would operate on the principle of adsorption. Adsorption phenomena require to develop a highly selective adsorbent for removing an adsorbate present in very small concentration (~10 ppm) in air streams. To that respect, silver-loaded zeolites are the subject of ongoing research because of their unique adsorption properties, coupled with the considerable hydrothermal stability of the Ag^+ cationic sites, which are particularly importants toward selective ethylene adsorption from mixtures of gases [12,13], and for air purification [14].

In the present work, an adsorptive approach for removing trace C_2H_4 from air streams using silver supported on microporous zeolites has been followed. With this purpose, a number of silver-containing zeolites, were prepared by a cation exchange method. After characterization of Ag-zeolite samples by XRD, XPS, HRTEM, UV-Vis and H_2-TPR, the impact of the zeolite framework on the state of the silver, and adsorption capacity based on π-complexation of C_2H_4 present in trace amounts are presented.

2. Experimental section

2.1. Materials and reagents

5A zeolite in powder form is commercially available from Sigma

---

Aldrich. NaY (CBV712) was obtained from Zeolyst International, and SSZ-13 [15], ITQ-29 [16], and SSZ-39 [15] were prepared according to literature procedures. Silver nitrate solution ($AgNO_3$) was purchased from Fluka international, and it was used as received.

2.2. Ion exchange method

Ag-zeolite samples were prepared by exchanging 1 g of zeolite, previously calcined in air at 550 °C for 12 h, with 100 ml of destilled and deionized water, and the corresponding quantity of 1 mM $AgNO_3$ solution. The mixture was stirred at room temperature in the dark for 24 h. Ag-zeolite samples were obtained by filtration, washed with deionized water, and acetone and dried in an oven at 100 °C overnight. Finally, Ag-zeolite samples were calcined at 350 °C with 1 °C min^{-1} ramp in a 50 ml min^{-1} of N_2 gas flow.

2.3. Characterization of the adsorbents

Elemental chemical analyses were performed by inductively coupled plasma atomic emission spectrometry (ICP-AES), using a Varian 710-ES spectrometer, after acid digestion of the samples in a mixture of $HNO_3/H_2O_2/HF$. Powder XRD were obtained with a Philips X'Pert diffractometer using the Cu-Kα radiation ($\lambda = 1.541874$ Å) at a scan rate of 2 min^{-1}. Textural properties were derived from the N_2 adsorption isotherms measured at -196 °C in ASAP-2420 Micromeritics equipment. Specific surface areas were calculated following the Brunauer-Emmett-Teller (BET) method. Total pore volumes (TPV) were determined at a relative pressure of 0.98, and pore size distributions were obtained by applying the Barrett-Joyner-Halenda (BJH) approach. Prior to the adsorption measurements, the samples were degassed at 300 °C and vacuum for 2 h. Thermal gravimetric analyses of the adsorbent samples were measured with a (TG/DT) analysis in a Mettler Toledo TGA/SDTA851e apparatus. Nanoparticle size was determined by high resolution transmission electron microscopy (HRTEM) using a JEM 2100F system with an operating voltage of 200 kV. TEM samples were prepared by placing microdrops of solution suspension directly onto a copper grid coated with carbon film. Diffusive reflectance UV-Vis spectra of adsorbents were measured by an UV0811M209 (Varian) equipment with the reference of $BaSO_4$.

Reducibility of silver was investigated by H_2-TPR using a Micromeritics Autochem 2910 apparatus. Samples were pretreated with 50 ml min^{-1} of Argon gas flow at 300 °C for 1 h and then cooled down to room temperature. After this procedure, the samples were heated from room temperature to 800 °C with 10 °C min^{-1} ramp in a 50 ml min^{-1} of 10% H_2/Ar mixture gas flow. The water formed during reduction with H_2 was trapped using a cold trap and the hydrogen consumption was continuously monitored with a TCD detector.

X-ray photoelectron spectras (XPS) were obtained in a SPECS spectrometer with a 150MCD-9 detector, using a non-monochromatic Mg Kα (1253.6 eV) X-ray source. Spectra were recorded using an analyzer pass energy of 30 eV, an X-ray power of 200 W, and an operating pressure of 10-9 mbar. Samples were analysed after N_2 pretreatment in vacuum at 300 °C in a micro-reactor directly connected to the UHV of the XPS analysis chamber. During XPS spectra data processing, binding energy (BE) values were referenced to the Si (2p) peak (103 eV). Spectra treatment was performed using the CASA software.

2.4. Breakthrough adsorption curve experiments

The breakthrough curves of trace ethylene adsorption in Ag-zeolite samples were measured in a fixed-bed adsorption column with 10 mm internal diameter, and inlet gas concentrations were equipped with humidity and CO_2 filters. The outlet gas was analysed by a gas chromatography Tracera GC-2010 Plus A (Shimadzu Co., Kyoto Japan) equipped with a barrier discharge ionization detector (BID) with 0.1 ppm detection limit. Experiments were done under the following

conditions: adsorbents were heated at 300 °C for 1 h in nitrogen to remove water and to clean the surface before adsorption. For each test, 5 mg of adsorbent was diluted with 200 mg of silicon carbide and loaded into the fixed-bed system. Breakthrough adsorption curves were measured at WHSV = 12000 $cm^3g_{ads}^{-1}h^{-1}$ of 10 ppm C_2H_4/10%O_2/N_2 at 0 °C and atmospheric pressure, and the flow rate of the mixture was maintained at 40 ml min^{-1} (normal temperature and pressure (NTP)) during adsorption process. When the effluent concentration of C_2H_4 reached the specified concentration, the experiment was stopped and C_2H_4 adsorption was calculated by integration of the C_2H_4 GC signal.

3. Results and discussion

3.1. Characterization of Ag-Zeolite samples

Ag exchanged zeolites with different framewroks (-CHA (SSZ-13), -LTA (5A, ITQ-29), -AEI (SSZ-39), and -FAU (Y)) were characterized by XRD and shown in Fig. 1. The diffractograms of Ag-zeolite samples after silver ion exchange were similar to the original zeolites (not shown) indicating that procedure for generating Ag-zeolite samples had no impact on zeolite cristallinity. Diffraction peaks related to formation of metallic silver particles were not detected by XRD.

Physico-chemical properties of silver zeolites are shown in Table 1. It can be seen there that, under our experimental conditions, 5A zeolite (Si/Al = 1) has similar amount of silver per unit cell than the other structures with higher Si/Al ratio, except Ag−Y sample that has a lower silver content (see Fig. S1 in supporting information) [17]. Textural properties of these samples are also shown in Table 1. Comparing Ag-5A and Ag-SSZ13 samples with those of the parent zeolite (without exchange), it can be seen that micropore volume decrease within the Ag exchanged samples. The smaller micropore volume could be explained due to the presence of small silver nanoparticles inside the cavities. Indeed, after the treatment at 300 °C, the formation of small Ag nanoparticles could be expected. HRTEM images presented in Fig. 2, show the typical morphology of the microporous zeolites, indicating that the crystallinities of parent zeolites were kept upon metal exchange and calcination procedures, in good agreement with XRD analyses. Ag nanoparticles with spherical shape were observed, and they present a face centered cubic crystal symmetry with an interplanar distance $d_1 = 0.235$ nm associated with (111) plane [18,19]. The size distributions of silver nanoparticles are shown in Fig. 2. Particle size histograms present silver particles with different average sizes and distributions depending on the zeolite used. In the case of -CHA, -AEI, -MOR and-LTA
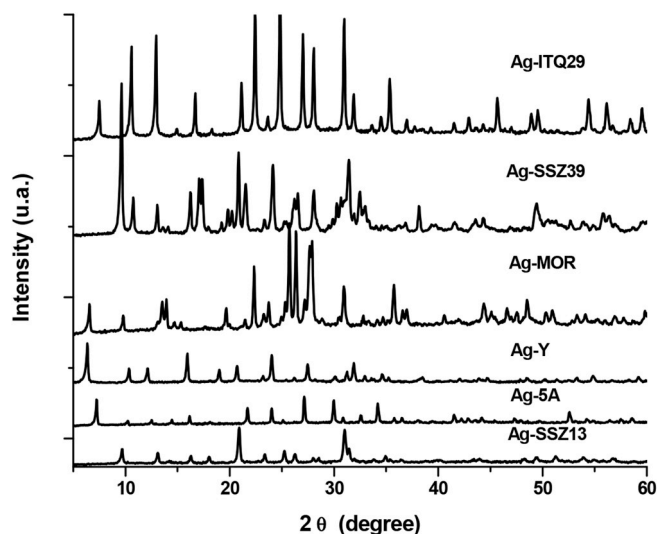

Fig. 1. XRD patterns of Ag-zeolite samples.

Table 1
Physico-chemical properties of Ag zeolites.

Sample	Framework Type	Si/Al[a]	Ag (%)[a]	BET ($m^2 g^{-1}$)	V_{micro} ($cm^3 g^{-1}$)
SSZ13	–CHA	6.0	–	566.85	0.257
Ag-SSZ13	–CHA	6.0	4.81	509.43	0.238
5A	–LTA	1.0	–	550.25	0.269
Ag-5A	–LTA	1.0	5.16	438.29	0.213
Ag-ITQ29	–LTA	5.0	4.36	554.08	0.244
Ag–Y	–FAU	5.5	2.43	517.87	0.215
Ag-SSZ39	–AEI	7.0	5.20	419.26	0.197
Ag-MOR	–MOR	6.3	8.59	240.94	0.110

[a] Measured by ICP.

frameworks, the mean diameter is between 2 and 3 nm and size distributions are similar for the four silver zeolite samples. In the case of Ag-FAU the particle size is much larger (< 10 nm) and also shows a broader particle size distribution. Notice that this does not exclude the presence of crystallites with sizes below 1 nm in the zeolite samples. It should also be considered that silver particle sizes observed by HRTEM may not be the original size of Ag in the samples, since metal agglomeration can occur due to the electron beam. Nevertheless, it can be said that the observed particle sizes are smaller in the 8R zeolites, while in the case of faujasite structure the Ag nanoparticles formed grew larger in size.

3.2. Breakthrough adsorption curves

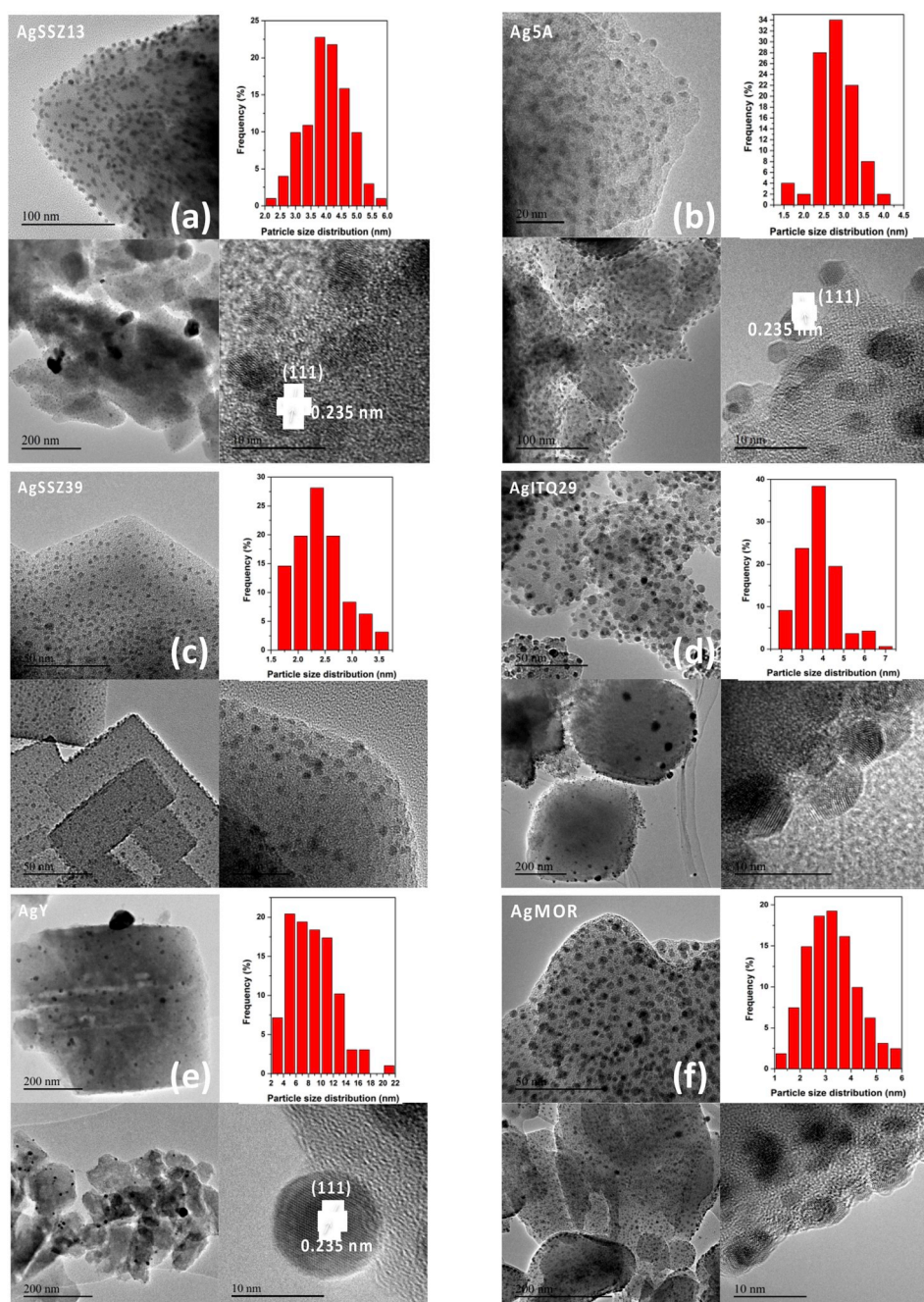Breakthrough curves of C_2H_4 adsorption on the SSZ-13 and 5A

Fig. 2. HRTEM images and particle size distribution of Ag-zeolites: a) Ag-SSZ13, b) Ag-5A, c) Ag-SSZ39, d) Ag-ITQ29, e) Ag–Y and f) Ag-MOR.
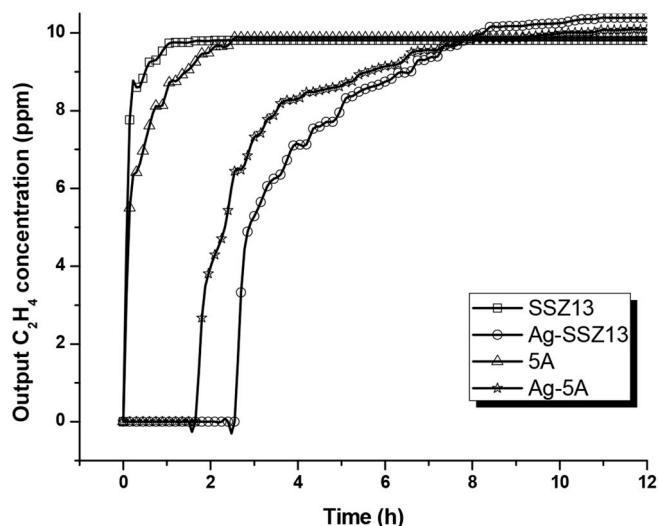
Fig. 3. Breakthrough profiles of C_2H_4 removal from 10 ppm $C_2H_4/10\%O_2/N_2$ stream at 0 °C, WHSV = 12000 $cm^3 \cdot g_{ads}^{-1} \cdot h^{-1}$

Fig. 4. Diffuse reflectance UV-Vis spectra of Ag-zeolite samples.

zeolites before and after Ag exchange are depicted in Fig. 3 (see breakthrough adsorption curves for the other samples in Fig. S2). The shape of the breakthrough curves is determined by both, hydrodynamic (axial dispersion) and kinetic (transport rates) factors. However, the breakthrough behavior is strongly dependent on the nature and type of adsorption isotherm. Firstly, the ethylene uptake capabilities of the parent zeolites (SSZ-13 and 5A) were examined, and they exhibit low ability to adsorb ethylene. This trend was improved by the introduction of Ag, being the adsorption capability significantly enhanced. Ethylene adsorption capacity was estimated to be 1.03 and 20.81 L Kg_{ads}^{-1} for the bare SSZ-13 and 5.0% Ag-SSZ13, respectively. A similar behavior was observed for the 5.0% Ag-5A sample with an estimated ethylene adsorption capacity of 17.3 L Kg_{ads}^{-1}. Breakthrough curves of both Ag-SSZ13 and Ag-5A are s-shaped, and the curves rise sharply at the breakthrough points indicating that the adsorbents can still effectively remove C_2H_4 with high purification efficiency (below 0.1 ppm), during 150 and 110 min, respectively. Ethylene can be absorbed within the zeolite by cation–π interaction which could occur between the π−electrons of C=C bond and positively charged metal species, and also by CH−O interaction between CH of ethylene and O of the zeolite framework [20]. Adsorption capacities of Ag-zeolite samples synthesized are shown in Table 2. According to these results, the best C_2H_4 adsorption capacity was obtained with Ag-SSZ13 and Ag-5A samples, indicating a higher ability of these two zeolites to form π-complexation bonds with olefins.

Table 2
Adsorption capacities of Ag-zeolite samples in C_2H_4 trace elimination.

Sample	Adsorption Capacity (L Kg_{ads}^{-1})[a]	Adsorption Capacity per metal (L g_{Ag}^{-1})[a]
SSZ-13	0.89	–
5A	1.54	–
Ag-SSZ13	20.81	0.433
Ag-5A	17.3	0.335
Ag-ITQ29	10.55	0.242
Ag-MOR	8.59	0.199
Ag-SSZ39	10.16	0.195
Ag−Y	2.88	0.119

[a] Adsorption conditions: 10 ppm $C_2H_4/10\%O_2/N_2$ at 0 °C, WHSV = 12000 $cm^3 \cdot g_{ads}^{-1} h^{-1}$.
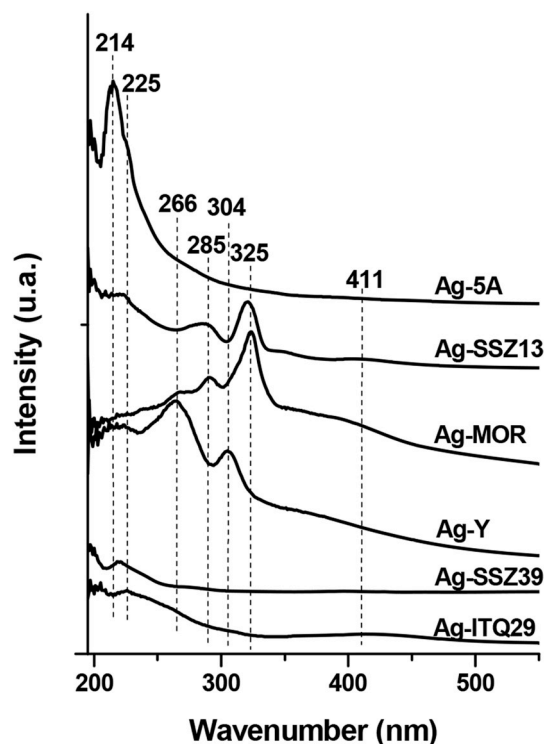
3.3. The nature of Ag species for adsorption of C_2H_4

In order to gain a better understanding of the π-complexation ability of the Ag-zeolites, diffuse reflectance UV-Vis experiments were performed. As show in Fig. 4, UV-Vis spectra indicate the existence of differents oxidation states of silver. Indeed, major bands at 214, 225, 266, 285, 304, 325, and 411 nm can be detected. According to previous reports [21–32], there is a general consensus to assigned the band at 208–238 nm to Ag^+ and the band above 350 nm to Ag^0. On the other hand, the distinction between Ag_n^{m+} and Ag_m is somewhat difficult (240–350 nm). From the results presented in Fig. 4, it can be said that silver clusters can be readily prepared with a size ranging from highly dispersed Ag^+ to few atoms with molecular-like electronic band structure (Ag_n^{m+}) within the different zeolites. Moreover, the broad band above 350 nm with peak center at 411 nm, assigned to the small metallic Ag particles located inside the zeolite cages or to larger Ag particles located on the outside surface, can be observed in the Ag−Y and Ag-MOR samples, which might be led to the poor C_2H_4 adsorption capacities.

Since, it is not possible to deny the possibility that UV-Vis radiation modifies Ag species into zeolites, we further explore the oxidation state of silver by X-ray photoelectron spectroscopy. The binding energies (BE) of the elements detected by XPS are summarized in Table 3. Low XPS resolution spectras reveal the presence of silver, oxygen, silicon and aluminum. Meanwhile, high-resolution XPS spectra show a peak in the Si 2p at 103 eV, the Al 2p region at 74.2–75.3 eV and the O 1s in the region of 532–532.6 eV. They can be associated with tetrahedral Si atoms present in the zeolite, such as SiO_4 and terminal Si−OH groups, aluminum from tetrahedral AlO_4 groups and oxygen atoms which are linked to the tetrahedral primary groups of the zeolite structure, respectively [33]. Fig. 5 shows the high resolution XPS spectras of Ag-zeolite samples in Ag 3d region, exhibiting two main peaks centered at 368.6–369.5 eV for Ag $3d_{5/2}$ and 374.7–375.6 eV for Ag $3d_{3/2}$. The $AgNO_3$ also has been used as a reference material due to the different conclusions existing in the literature on the assignation of binding energies to different silver species [34–36]. It can be seen that the Ag $3d_{5/}$

Table 3

Binding energies (BE) from the high XPS resolution spectra in the Si 2p, Al 2p, O 1s and Ag 3d region of the samples.

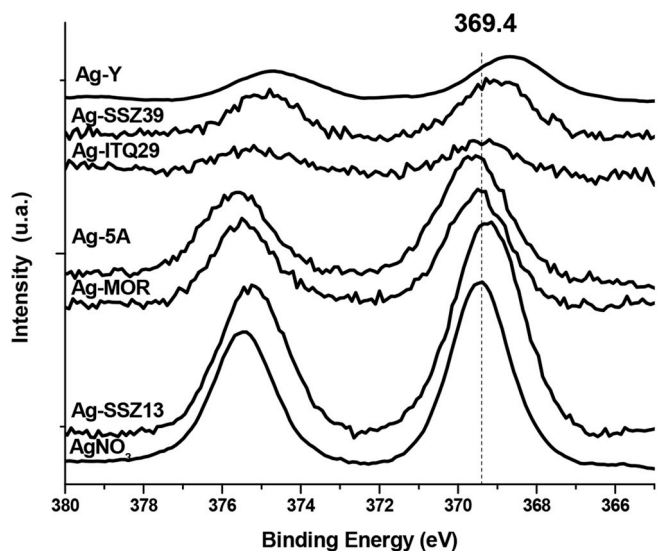| Sample	Binding energy (eV)				
	Si 2p	Al 2p	O 1s	Ag 3d $_{5/2}$	Ag 3d $_{3/2}$
AgNO$_3$	–	–	–	369.4	375.4
Ag−Y	103	74.6	532.5	368.6	374.7
Ag-5A	103	75.3	532.0	369.5	375.6
Ag-SSZ13	103	74.2	532.5	369.2	375.2
Ag-ITQ29	103	75.0	532.6	369.5	375.4
Ag-SSZ39	103	74.5	532.3	369.0	374.9
Ag-MOR	103	74.5	532.5	369.5	375.5

Fig. 5. High resolution spectra of Ag 3d region for Ag-zeolite samples.

$_2$ of AgNO$_3$ locating at 369.4 eV can be associated with a major presence of highly dispersed Ag$^{\delta+}$ species [37]. Accordingly, Ag-SSZ13, Ag-5A, Ag-ITQ29 and Ag-MOR spectra could be associated with the presence of Ag$^{\delta+}$ nanoclusters and nanoparticles. While, the peak at 368.6 eV in Ag−Y spectra suggests the presence of silver metal particles [37]. This result is consistent with the previously reports that Ag$^+$ ions in Ag−Y could be easily reduced to bulk silver clusters, and metallic silver particles on the external surface of the zeolite, severely deactivating the π-complexation in ethylene adsorption [35,38]. Indeed, while silver oxides have been reported to form strong π-complexation bonds with olefins through the donation of olefin π-bond electrons to the empty s-orbital of the metal and the d-π* back donation, metallic silver with a partially filled 5s orbital can not gain electrons from the π-bond of ethylene to form π-complexes [39]. Taking this into account, the low ethylene adsorption capacity showed in the Ag−Y sample can be related to the reduction of Ag$^{\delta+}$ species to Ag^0 in good agreement with UV-Vis and XPS results.

At this point, and in order to confirm and quantify the role of the Ag$^{\delta+}$ species in ethylene adsorption, H$_2$-TPR measurements were carried out. The H$_2$-TPR profiles normalized by Ag amount are shown in Fig. 6. No hydrogen consumption was observed in the blank experiment with bane zeolites, while all Ag-zeolite samples contain reducible Ag$^{\delta+}$ species, as can be seen from TPR experiments. Reduction of Ag$^{\delta+}$ species was complete at 450 °C for Ag-SSZ13 sample. The three maxima observed in the H$_2$-TPR curves may indicate the presence of different Ag$^{\delta+}$ species. The main hydrogen consumption, centered at 129 °C is attributed to the reduction of Ag$^+$ ions, while the peak at 196 °C has been assigned to the reduction of Ag$_n^{m+}$ clusters [40,41]. The third hydrogen consumption peak, might be associated with residual AgNO$_3$

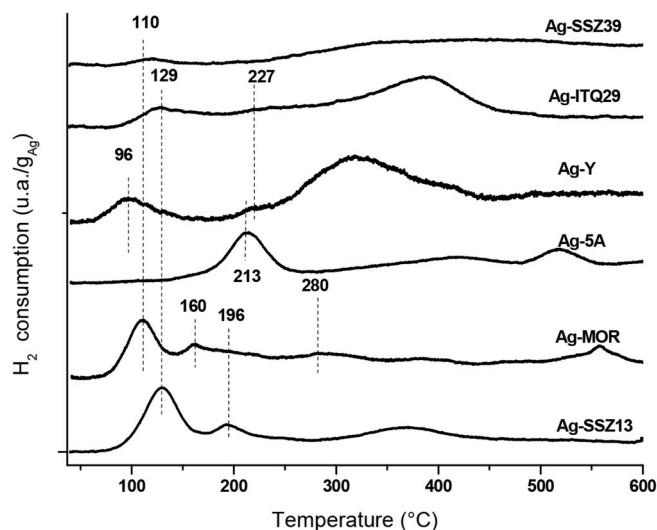**Fig. 6.** H$_2$-TPR profiles of Ag-zeolite samples.

reduced at higher temperature in good agreement with TG experiments (not shown). In Ag−Y sample, the reduction of Ag$^{\delta+}$ species started at the lowest temperature (ca. 96 °C) [40–42]. This results can be explained assuming that not only Ag$^+$ concentration but also the presence of Ag^0 has an influence on the kinetics of reduction, as has been shown by Beyer et al. in their studies on the kinetics of the reduction of Ag$^+$ in Y zeolites [40]. On the contrary, Ag-5A sample presented the most stable Ag$^{\delta+}$ species, which are reduced at 213 °C. By comparing spectras, the presence of Ag$^{\delta+}$ species appear to be favoured in Ag-SSZ13 and Ag-5A samples, while Ag−Y sample shows the lowest intensity of this species in good agreement with the UV-Visible and XPS results presented before.

Quantitative results of the TPR profiles are summarized in Table 4, and a fair correlation between H$_2$ consumption attributed to Ag$^{\delta+}$ species and C$_2$H$_4$ adsorption capacity per metal center could be deduced from Fig. 7. The higher ability to form π−complexes in Ag-SSZ13 and Ag-5A samples, could be explained by the good stabilization of highly dispersed Ag$^{\delta+}$ species in these two zeolites [43]. On the contrary, low C$_2$H$_4$ adsorption capacities of Ag−Y and Ag-MOR samples can be associated with the low stability of Ag$^{\delta+}$ species in these structures with preferential formation of Ag^0. This in turn confirms that the contribution of Ag^0 for trace C$_2$H$_4$ elimination by adsorption is considerably less important compared with Ag$^{\delta+}$ species.

4. Conclusions

Ethylene adsorbents containing well dispersed Ag$^{\delta+}$ species in differents zeolite framework have been prepared. Our results shown that the zeolite structure plays an important role on the stabilization of silver cationic species and therefore in C$_2$H$_4$ adsorption capacity. Smaller particle size and narrow particle size distributions were obtained using zeolites with 8R. Trace ethylene adsorption experiments combined with characterization of Ag-zeolite samples have elucidated different silver species present in the zeolites and their role on C$_2$H$_4$

Table 4

Quantitative results on hydrogen consumption obtained by TPR experiments.

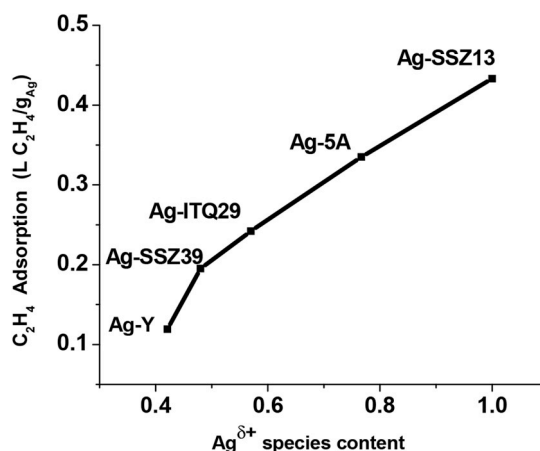| Sample	H$_2$ consumption (ml/g STP)	Normalized Ag$^{\delta+}$ content
Ag-SSZ13	11.11	1
Ag-5A	8.49	0.76
Ag-ITQ29	6.33	0.57
Ag-SSZ39	5.33	0.48
Ag−Y	4.68	0.42

Fig. 7. Correlation between $Ag^{\delta+}$ species content and C_2H_4 adsorption capacity per metal center into Ag-zeolite samples.

adsorption. XPS and H_2-TPR results suggest that the contribution of Ag^0 in trace C_2H_4 elimination is less significant compared with $Ag^{\delta+}$ species, establishing a reliable correlation between the concentration of $Ag^{\delta+}$ species and trace ethylene adsorption capacity. Finally, the most relevant trace ethylene adsorption capacity of the Ag-SSZ13 and Ag-5A samples are associated with an excellent stabilization of $Ag^{\delta+}$ species into the pores. Silver on chabazite shows a clear potential application for the efficient elimination of trace ethylene during transport or warehouse storage at 0 °C.

Acknowledgements

Appendix A. Supplementary data

Supplementary data to this article can be found online at https://doi.org/10.1016/j.micromeso.2019.03.032.

References

[1] M.E. Saltveit, Postharvest Biol. Technol. 15 (1999) 279–292.
[2] A.A. Kader, Hortscience 38 (2003) 1004–1008.
[3] J. Wojciechowski, G.D. Blanpied, J.A. Bartsh, J.M. Blankenship (Ed.), Proceedings of 4th National Controlled Atmosphere Research Conference, 1985 Raleight, North Caroline.
[4] J. Wojciechowski, M. Herregods (Ed.), International Symposium on Postharvest Handling of Fruit and Vegetables, vol 258, ISHS, Luewen, Belgium, 1989, p. p131. Acta Hortic. (Wagening.).
[5] A. El Blidi, L. Rigal, G. Malmary, J. Molinier, L. Torres, Food Qual. Prefer. 4 (1993) 119–126.
[6] J. Wojciechowki, J. Haber, Appl. Catal. 4 (1982) 275–280.
[7] J. Li, C. Ma, X. Xu, J. Yu, Z. Hao, S. Qiao, Environ. Sci. Technol. 42 (2008) 8947–8951.
[8] H.K. Hirayama and K. Sakurai, EP0914864A3, 2000/28.
[9] C.Y. Ma, Z. Mu, J.J. Li, Y.G. Jin, J. Cheng, G.Q. Lu, Z.P. Hao, S.Z. Qiao, J. Am. Chem. Soc. 132 (2010) 2608–2613.
[10] W.J. Xue, Y.F. Wang, P. Li, Z.-T. Liu, Z.P. Hao, C.Y. Ma, Catal. Commun. 12 (2011) 1265–1268.
[11] C. Jiang, K. Hara, A. Fukuoka, Angew. Chem. Int. Ed. 52 (2013) 6265–6268.
[12] S. Aguado, G. Bergeret, C. Daniel, D. Farrusseng, J. Am. Chem. Soc. 134 (2012) 14635–14637.
[13] R.T. Yang, E.S. Kikkinides, AIChE J. 41 (1995) 509–517.
[14] Q.H. Trinh, S.B. Lee, Y.S. Mok, J. Hazard Mater. 285 (2015) 525–534.
[15] N. Martín, Z. Li, J. Martínez-Triguero, J. Yu, M. Moliner, A. Corma, Chem. Commun. 52 (2016) 6072–6075.
[16] A. Corma, F. Rey, J. Rius, M.J. Sabater, S. Valencia, Nature 431 (2004) 287–290.
[17] H. van Bekkum, E. M. F., Introduction to Zeolite Science and Practice, Stud. Surf. Sci. Catal. (1991) Elsevier, Amsterdam.
[18] E. Rodríguez-León, R. Iñiguez-Palomares, R.E. Navarro, R. Herrera-Urbina, J. Tánori, C. Iñiguez-Palomares, A. Maldonado, Nanoscale Res. Lett. 8 (2013) 318.
[19] M.I. Mendivil, B. Krishnan, F.A. Sanchez, S. Martinez, J.A. Aguilar-Martinez, G.A. Castillo, D.I. Garcia-Gutierrez, S. Shaji, Appl. Phys. A 110 (2013) 809–816.
[20] N. Patdhanagul, T. Srithanratana, K. Rangsriwatananon, S. Hengrasmee, Microporous Mesoporous Mater. 131 (2010) 97–102.
[21] J. Shibata, Y. Takada, A. Shichi, S. Satokawa, A. Satsuma, T. Hattori, J. Catal. 222 (2004) 368–376.
[22] J. Texter, T. Gonsiorowski, R. Kellerman, Phys. Rev. B 23 (1981) 4407–4418.
[23] A. Keshavaraja, X. She, M. Flytzani-Stephanopoulos, Appl. Catal. B Environ. 27 (2000) L1–L9.
[24] E. Gachard, J. Belloni, M.A. Subramanian, J. Mater. Chem. 6 (1996) 867–870.
[25] P. Mulvaney, A. Henglein, J. Phys. Chem. 94 (1990) 4182–4188.
[26] T. Linnert, P. Mulvaney, A. Henglein, H. Weller, J. Am. Chem. Soc. 112 (1990) 4657–4664.
[27] G.A. Ozin, F. Hugues, J. Phys. Chem. 87 (1983) 94–97.
[28] J. Shibata, K.-I Shimizu, Y. Takada, A. Shichi, H. Yoshida, S. Satokawa, A. Satsuma, T. Hattori, J. Catal. 227 (2004) 367–374.
[29] K.A. Bethke, H.H. Kung, J. Catal. 172 (1997) 93–102.
[30] N. Bogdanchikova, F.C. Meunier, M. Avalos-Borja, J.P. Been, A. Pestryakov, Appl. Catal. B Environ. 36 (2002) 287–297.
[31] M. Richter, U. Bentrup, R. Eckelt, M. Schneider, M.-M. Pohl, R. Fricke, Appl. Catal. B Environ. 51 (2004) 261–274.
[32] B. Dong, R. Retoux, V. de Waele, S.G. Chiodo, T. Mineva, J. Cardin, S. Mintova, Microporous Mesoporous Mater. 244 (2017) 74–82.
[33] L. Ferreira, A.M. Fonseca, G. Botelho, C. Almeida-Aguiar, I.C. Neves, Microporous Mesoporous Mater. 160 (2012) 126–132.
[34] J.T. Wolan, G.B. Hoflund, Appl. Surf. Sci. 125 (1998) 251–258.
[35] A. Jayaraman, R.T. Yang, C.L. Munson, D. Chinn, Ind. Eng. Chem. Res. 40 (2001) 4370–4376.
[36] J. Padin, R.T. Yang, Chem. Eng. Sci. 55 (2000) 2607–2616.
[37] M. Richter, M. Langpape, S. Kolf, G. Grubert, R. Eckelt, J. Radnik, M. Schneider, M.-M. Pohl, R. Fricke, Appl. Catal. B Environ. 36 (2002) 261–277.
[38] K. Tsutsumi, H. Takahashi, Bull. Chem. Soc. Jpn. 45 (1972) 2332–2337.
[39] Q.H. Trinh, Y.S. Mok, Catal. Today 256 (2015) 170–177.
[40] H. Berndt, M. Richter, T. Gerlach, M. Baerns, J. Chem. Soc., Faraday Trans. 94 (1998) 2043–2046.
[41] H.K. Beyer, P.A. Jacobs, Stud. Surf. Sci. Catal. 12 (1982) 95–102.
[42] H. Beyer, P.A. Jacobs, J.B. Uytterhoeven, J. Chem. Soc., Faraday Trans. 72 (1976) 674–685.
[43] J. Zhou, Y. Zhang, X. Guo, A. Zhang, X. Fei, Ind. Eng. Chem. Res. 45 (2006) 6236–6242.